Identification of the Pyroptosis-related Signature for Predicting Prognosis in Cervical Cancer

Cankun Zhou
Southern Medical University Affiliated Maternal & Child Health Hospital of Foshan
https://orcid.org/0000-0002-7253-6686

Chaomei Li
Southern Medical University Affiliated Maternal & Child Health Hospital

Yuhua Zheng (yuhuazhengcn@gmail.com)
Southern Medical University Affiliated Maternal & Child Health Hospital of Foshan
https://orcid.org/0000-0002-0977-5115

Xiaochun Liu
Southern Medical University Affiliated Maternal & Child Health Hospital of Foshan

Research article

Keywords: Cervical cancer, Pyroptosis, Prognosis, Tumor microenvironment, Immune infiltration

Posted Date: September 30th, 2021

DOI: https://doi.org/10.21203/rs.3.rs-870182/v1

Version of Record: A version of this preprint was published at Aging on November 27th, 2021. See the published version at https://doi.org/10.18632/aging.203716.

Abstract

Background: Cervical cancer (CC) is one of the most common malignancies in gynecology. There is still a lack of specific biomarkers for the diagnosis and prognosis of CC. Pyroptosis is one of the methods of programmed cell death, and its various components are related to the occurrence, invasion, and metastasis of tumors. However, the role of pyroptosis in CC has not yet been elucidated.

Methods: This study focuses on the development of a prognostic signature associated with pyroptosis for CC patients using integrated bioinformatics to elucidate the relationship between the signature and the tumor microenvironment and immune response.

Results: We identified a prognostic signature based on eight pyroptosis-related genes (PRGs), with better prognostic survival in the low-risk group ($P<0.05$) and AUC values greater than 0.7. The results of the multi-factor Cox regression analysis indicated that the signature could be used as an independent prognostic factor, and both the DCA and the Nomogram suggested that the prognostic signature had good predictive power. Interestingly, this prognostic signature can also be applied to multiple tumors. In addition, the tumor microenvironment and immune infiltration status were significantly different between high and low-risk groups ($P<0. 05$). The core gene GZMB was screened and the CC-associated GZMB/ miR-378a/TRIM52-AS1 regulatory axis was constructed.

Conclusion: The study successfully established the prognostic signature based on eight PRGs and reflected their tumor microenvironment and immune infiltration. The GZMB/ miR-378a/TRIM52-AS1 regulatory axis may play an important regulatory role in the development of CC, and further experimental studies are needed to validate these results subsequently.

Introduction

Cervical cancer (CC) is the 4th most common malignancy among women worldwide(1). While the incidence and mortality rates of cervical cancer have declined significantly in high-income countries, the overall prognosis for CC patients in low-income countries remains poor(2, 3). And in the event of recurrence and metastasis, the patient's prognosis is further reduced, so cervical cancer will remain a heavy burden of disease for a long time to come. Therefore, further exploration of the molecular mechanisms underlying the development of cervical cancer is crucial, and striving for early diagnosis and treatment is essential to improve the survival rate of CC patients.

Cell death is mainly divided into two categories, namely programmed death and non-programmed death. Programmed death mainly includes apoptosis, pyroptosis, and necroptosis, and non-programmed death mainly includes cell necrosis. Different from apoptosis or necrosis, pyroptosis is a kind of programmed death mediated by caspase and inflammasomes, characterized by rapid plasma membrane rupture followed by the release of cellular contents and pro-inflammatory substances such as IL, triggering an inflammatory cascade that causes cellular damage(4). Pyroptosis not only plays an important role in infectious diseases, cardiovascular diseases, and central nervous system diseases but is also closely

related to tumors(5). For tumors, it is a double-edged sword. On the one hand, as an intrinsic immune mechanism, pyroptosis inhibits the occurrence and development of tumors. On the other hand, as a form of pro-inflammatory cell death, it provides a suitable microenvironment for tumor growth. The key components of the pyroptosis, such as inflammatory vesicles, gasdermin proteins and pro-inflammatory cytokines, are associated with the occurrence, invasion and metastasis of tumors(6, 7). Meanwhile, previous studies have found that HeLa cells overexpressing GSDMB exhibit significant pyroptosis characteristics(8). In addition, immune cells promote HeLa pyroptosis by releasing GZMB and lysing GSDME(9). In human papillomavirus (HPV)-positive cells, the expression of IL-1β, an important inflammatory molecule in the process of pyroptosis, was completely inhibited, thus blocking the containment of tumor cells by pyroptosis. Meanwhile, the expression of SIRT1 in cervical cancer cells affected the stability of RelB mRNA, which in turn affected the expression of AIM2. When SIRT1 was knocked down, the stability of RelB was significantly enhanced and the expression of AIM2 inflammation-related genes was significantly up-regulated, triggering AIM2 inflammation vesicle-mediated pyroptosis(10, 11). However, the characterization and prognostic value of PRGs for cervical cancer has not yet been elucidated.

In this study, we analyzed the genetic data of cervical cancer in the TCGA (The Cancer Genome Atlas) database to describe the expression levels and genetic changes of PRGs, and constructed and validated a prognostic model based on CC samples, and screened out core genes and pan-cancer analysis.

Methods

Datasets and preprocessing

The TCGA database (https://portal.gdc.cancer.gov/) and the UCSC Xena database (http: //www. Xebabrowser.net) were used to obtain CC data. The RNA sequence data, clinicopathological parameters, and genomic mutation data (including somatic mutations and copy number variants (CNV)) were obtained for 306 CC tissues and 3 paraneoplastic tissue samples. Based on previous studies(9, 12, 13), 35 PRGs were included, namely AIM2, CASP1, CASP3, CASP4, CASP5, CASP6, CASP8, CASP9, ELANE, GPX4, GSDMA, GSDMB, GSDMC, GSDMD, GSDME, GZMA, GZMB, IL18, IL1B, IL6, NLRC4, NLRP1, NLRP2, NLRP3, NLRP6, NLRP7, NOD1, NOD2, PJVK, PLCG1, PRKACA, PYCARD, SCAF11, TIRAP, TNF, as detailed in Supplementary Table 1. Comparison of mRNA expression levels of PRGs in paraneoplastic tissue and CC tissues, and visualization of somatic mutations and copy numbers in CC tissues by the R software 'maftools' and the 'Rcircos' package. The Kaplan Meier-Plotter online platform (https://kmplot.com/analysis/) was used to further analyze the survival and prognosis of PRGs(14). All subsequent statistical analyses were implemented with R version 4.0.2. The screening criterion for differential expression of PRGs was $P<0.05$.

Establishment of the prognostic signature

To screen for prognosis-related PRGs and to exclude samples with no survival time, 304 CC patients in the TCGA database were used as the training dataset. We constructed a prognostic signature for PRGs using univariate Cox proportional regression analysis and least absolute shrinkage and selection operator (Lasso) regression, stratified according to the risk score (Risk score = $EXP_{PRGs\ 1} * Coefficient_1 + EXP_{PRGs\ 2} * Coefficient_2 + ... + EXP_{PRGs\ n} * Coefficient_n$), and the associated risk score was calculated for each patient in the training dataset. Based on the median score, the groups were classified as low or high risk. The difference in survival between the two groups was assessed using the log-rank test and Kaplan-Meier curves, and the sensitivity and specificity of the prognostic signature were assessed by plotting ROC curves using the 'survivalROC' package. To determine the feasibility and reliability of our prognostic signature for PRGs, the training dataset of CC patients (N = 304) was randomly divided into test dataset A (N = 152) and test dataset B (N = 152) using the "Caret" package, and the same statistical methods were used in both test datasets for validation.

Then, independent prognostic analyses and decision curve analysis (DCA) were performed to combine the clinical feature, and a nomogram was constructed to predict the 1-, 3- and 5-year survival rates of CC patients to assess the prognostic value of the signature.

Obtain TCGA pan-cancer transcriptional expression data and clinical data from the Xena database, including 33 cancer types, as detailed in Supplementary Table 2. The prognostic model was applied to the remaining 32 tumors to analyse their prognostic outcomes across the different cancers. The risk score was considered to be significantly associated with CC patient survival when $p<0.05$.

Tumor mutation burden, tumor microenvironment, and Immune cell infiltration analysis

Tumor mutation burden (TMB) as a biomarker can help predict a patient's response to immunotherapy(15). TMB differences between the high and low-risk groups were compared based on the original data of somatic mutations in CC patients, and the association between risk scores and TMB was assessed using Spearman correlation analysis. The ESTIMATE algorithm was used to predict the purity of the CC(16), and the proportion of stromal cells (stromal score) and immune cells (immune score) infiltrated in the tumor tissue, and the differences in the tumor microenvironment (TME) between the two risk groups were assessed.

Immune cell infiltration data from CC were downloaded via the Timer 2.0 database (http://timer.cistrome.org/)(17). Four algorithms were eventually included(18-20), including TIMER, CIBERSORT, QUANTISEQ, and MCPCOUNTER, based on the pyroptosis-related signature, and the correlation between the immune cell infiltration and risk score under different algorithms was analyzed using Spearman correlation, shown in a bubble plot. In addition, differences in immune function, HLA gene expression, immune checkpoint, and m6A gene expression were further compared between the high and low-risk groups using the Wilcox test. P□0.05 was considered to be statistically significant.

Construction of ceRNA interoperability network

To screen for core genes in the prognostic signature, we searched for protein-protein interactions (PPI) through the String (https://string-db.org/) online database, searched for interactions between proteins. We also counted the degree of connectivity of these PRGs. Next, the genes in the prognostic signature were evaluated for correlation with the clinical feature Grade. Patients were divided into two subgroups, G1-2 and G3-4, and the Wilcox test was used for analysis. The genes with the highest connectivity and statistically significant correlation with the Grade in the signature were set as core genes.

To construct the mRNA-miRNA-LncRNA interaction network for the core genes, the miRNAs targeted by the core genes were predicted using the databases TargetScan (http://www.targetscan.org/vert_72/) and miRTarBase (http://mirtarbase.cuhk.edu.cn/). The predicted miRNAs were intersected, and the differential expression levels and prognostic values of these miRNAs were analyzed.

Based on the prognostic value and differentially expressed miRNAs, LncBase Predicted v.2 (https://carolina.imis.athena-innovation.gr/diana_tools/web/index.php? r=lncbasev2/index -predicted) and StarBase (http://starbase.sysu.edu.cn/) to predict the LncRNAs that the miRNAs might bind. Finally, we further analyzed the differential expression levels and prognostic value of these LncRNAs and constructed mRNA-miRNA-LncRNA interactions networks. The statistically significant difference was $P < 0.05$.

Results

Genetic variation profile of the PRGs in CC

First of all, we found that AIM2, CASP3, CASP4, CASP5, CASP6, CASP8, GSDMB, GSDMC, GZMB, IL18, NLRP2, NLRP7, NOD2, PYCARD, and TNF were significantly upregulated in CC tissues, while ELANE, NLRP1, NOD1, and PJVK were significantly downregulated (Fig 1A). Survival prognosis analysis showed that IL 1B and PRKACA were significantly correlated with the prognosis of CC patients. The patients with low expression of IL 1B and high expression of PRKACA have a better survival prognosis (Fig 2B/C). Fig 2D shows the location of CNV alterations on chromosomes in PRGs, and that CNV changes were prevalent in these genes, with PRKACA having the highest probability of CNV amplification and GPX4 having the highest frequency of CNV deletion (Fig 1E). We also analyzed the somatic mutations of these PRGs in CC and showed that the overall mutation frequency was not high (≤4%) (Fig 1F).

Construction and evaluation of the effectiveness of prognostic signature

We performed a survival analysis of PRGs in the training dataset using a univariate Cox proportional regression model and screened for eight PRGs with prognostic value (Fig 2A), of which GZMB and TNF

were significantly highly expressed in CC tissue and NOD1 was significantly low (Supplementary Fig 1B). Next, the pyroptosis-related signature was constructed by further downscaling the prognosis-related PRGs through Lasso regression (Fig 2B-C), and the risk score was calculated for each patient, risk score== $(-0.0037\times EXP_{GPX4}) + (0.0377\times EXP_{GSDME}) + (-0.0043\times EXP_{GZMA}) + (-0.026\times EXP_{GZMB}) +(0.0017\times EXP_{IL1B}) + (0.4741\times EXP_{NOD1}) + (-0.1298\times EXP_{PRKACA}) + (0.0642\times EXP_{TNF})$. Based on the median, patients were divided into low-risk and high-risk groups, and survival prognostic analysis showed a significant survival benefit for patients in the low-risk group ($P < 0.001$, Fig 3A), its AUC was 0.789. In test dataset A and test dataset B, the difference in survival prognosis ($P < 0.05$, Fig 3B/C) and predictive efficacy (AUC were 0.707 and 0.943, respectively, Fig 3E/F) were similarly validated, confirming the overall accuracy and validity of the prognostic signature. Interestingly, this prognostic model showed a better prognosis for patients in the low-risk group than in the high-risk group in Glioblastoma multiforme (GBM), Brain Lower Grade Glioma (LGG), Liver hepatocellular carcinoma (LIHC), and Uterine Corpus Endometrial Carcinoma (UCEC) (Supplementary Fig 2).

Univariate and multivariate COX analyses combined with patient Age, Stage, Grade, showed that the pyroptosis-related signature was an independent prognostic factor for OS in CC patients ($p < 0.001$, Fig 4A/B). In addition, the risk score had the highest AUC value (AUC=0.794, Fig 4C) compared to other clinical features, and the DCA further demonstrated the clinical usefulness of the signature (Fig 4D). The Nomogram for both the signature and clinical features is stable and accurate and can be used to predict 1-year, 3-year, and 5-year survival rates in CC patients (Fig 4E).

Correlation of TMB, TME, and Immune cell infiltration with the prognostic signature

Previous studies have reported an important role for the TME in the occurrence and development of tumors(21). Given that TMB predicts patient response to immunotherapy, our study found that patients in the high-risk group were accompanied by low TMB scores, and the risk score was significantly negatively correlated with TMB score. The results of the survival analysis showed that patients with high-risk scores combined with low TMB scores showed a significant survival advantage (Fig 7A-C). Compared to the high-risk group, ESTIMATEScore, ImmuneScore, and StromalScore were all higher in the low-risk group (Fig 7D).

The relationship between immune response and risk score based on the TIMER, QUANTISEQ, MCPCOUNTER, and CIBERSORT algorithms is shown in Fig 5E. The risk score was negatively related to the infiltration level of B cell, T cell CD8+, Macrophages, and positively to the infiltration level of Neutrophils. The analysis of immune function differences showed that antigen-presenting cell (APC) co-inhibition/ APC_co_stimulation, CC chemokine receptor (CCR), Check-point, Cytolytic_activity, human leukocyte antigen (HLA), Inflammation promoting, T cell co inhibition/ stimulation were significantly more active in the low-risk group (Fig 6 A).

In the view of the above analysis of immune function, differences showed significant differences in HLA between the two groups, HLA-related gene expression levels were further analyzed as shown in Fig 6 B. HLA-DMA, HLA-DQB1, HLA HLA-DMA, HLA-DQB1, HLA-DQB1, HLA-DRA, etc. were significantly higher in the low-risk group. Due to the importance of immunotherapy with checkpoint inhibitors, we further analyzed the differences in immune checkpoint expression between the two groups and showed significant differences in the expression of PDCD1LG2, TMIGD2, CD27, CD40LG, etc. between the two groups (Fig 6C). The latest research suggests that m6A can regulate immune response and participate in the regulation of the tumor immune microenvironment(22). Comparison of m6A-related mRNA expression between high and low-risk groups showed that YTHDF3, LRPPRC were significantly more highly expressed in the high-risk group (Fig 6D).

Construction of core gene ceRNA interoperability network

The interrelationships between the 35 PRGs included in this study were retrieved from the STRING database and a PPI network was constructed with a composite score of >0. 4. A close and complex network of interrelationships was found between these genes (Supplementary Fig 3A). And count the degree of connectivity between these genes (Supplementary Fig 3B). We further analyzed the relationship between mRNA expression levels in the pyroptosis-related signature and CC Grade staging and found that GPX4, GZMA, and GZMB expression was significantly higher in the G3-4 group compared to the G1-2 group ($P < 0.05$, Supplementary Fig 3C/E/F). The connectivity of GPX4, GZMA, and GZMB in the above PPI network was 4, 4, and 10, respectively, suggesting that GZMB may be involved in the tumor progression of CC.

Further pan-cancer expression analysis was performed for GZMB, showing significant high expression of GZMB in Cholangiocarcinoma (CHOL), Colon adenocarcinoma (COAD), Esophageal carcinoma (ESCA), Glioblastoma multiforme (GBM), Head and Neck squamous cell carcinoma (HNSC), Kidney renal clear cell carcinoma (KIRC), Rectum adenocarcinoma (READ), Stomach adenocarcinoma (STAD), and Uterine Corpus Endometrial Carcinoma (UCEC) tissues and significant low expression in Lung adenocarcinoma (LUAD) and Lung squamous cell carcinoma (LUSC) tissues (Fig 7A). And prognostic correlation analysis showed that GZMB was negatively correlated with survival in Bladder Urothelial Carcinoma (BLCA), Breast invasive carcinoma (BRCA), Cervical squamous cell carcinoma and endocervical adenocarcinoma (CESC), Ovarian serous cystadenocarcinoma (OV), Skin Cutaneous Melanoma (SKCM), UCEC, and Uveal Melanoma (UVM), while it was positively correlated with GBM, KIRC, Kidney renal papillary cell carcinoma (KIRP), Acute Myeloid Leukemia (LAML), and Brain Lower Grade Glioma (LGG) ($P<0.05$, Fig 7B). To clarify the potential molecular regulation mechanism of GZMB in CC, we further constructed an mRNA-miRNA-LncRNA interaction network. First, based on the comprehensive prediction of TarBase and mirTarBase databases, we screened out miRNAs that can target and regulate the core gene GZMB, and subsequently, 10 miRNAs were obtained by taking the intersection (Fig 7C). Further analysis showed that miR-378a was significantly upregulated in CC (Fig 7D) and its high expression patients have a better prognosis for survival (Fig 7E). The LncRNA targets upstream of miR-

378a were obtained from the LncBase and StaBase databases, and a total of 5 LncRNAs (Fig 7F) were obtained by taking the intersection to finally construct the mRNA-miRNA-LncRNA interactions network (Fig 7I). Next, these five LncRNAs were also subjected to differential expression analysis and survival prognosis analysis, which showed that TRIM52-AS1 was significantly downregulated in CC (Fig 7G), and its high expression level showed a significant survival advantage (Fig 7H). Thus, the GZMB - miR-378a - TRIM52-AS1 regulatory axis may play an important regulatory role in the development of CC.

Discussion

Pyroptosis is a novel form of programmed cell death, which plays a two-way role in the occurrence and development of tumors. It can regulate cell morphology, proliferation, infiltration, migration, and chemotherapy resistance through a variety of cell signaling pathways, thereby influencing tumor progression, and may be associated with patient prognosis(5). However, the regulatory mechanisms and networks between pyroptosis and CC are not fully understood. Our study aims to elucidate this aspect and provide new research ideas for its intervention.

In terms of gene expression, we first found that AIM2, CASP3, CASP4, CASP5, CASP6, CASP8, GSDMB, GSDMC, GZMB, IL18, NLRP2, NLRP7, NOD2, PYCARD, and TNF were mainly up-regulated in CC tissues, while ELANE, NLRP1, NOD1, and PJVK were mainly down-regulated. Among these, CC patients with low IL 1B expression and high PRKACA expression had poorer survival rates. This is consistent with previous findings finding that these important PRGs are closely associated with tumor development. In cervical, gastric and colorectal cancers, high IL-1B expression is associated with shorter patient survival(23, 24). In addition, IL-1β expression was also elevated in prostate cancers with a high propensity to metastasize(25). In a study of head and neck tumors, Dong et al. found a significant increase in lymph node metastasis with increased IL-1β expression(26), suggesting that high IL1B expression is detrimental to the survival of tumor patients. Many studies have shown that PRKACA plays an important role in the development and progression of a variety of cancers(27), and it has been postulated that PRKACA can be used as a biomarker for hepatocellular carcinoma(28). Therefore, these genes may be new molecular targets for CC.

In ovarian cancer and gastric cancer, researchers have carved out PRGs and constructed and validated prognostic models for PRGs(13, 29). Therefore, we constructed the pyroptosis-related signature consisting of eight PRGs with prognostic value (GPX4, GSDME, GZMA, GZMB, IL1B, NOD1, PRKACA, TNF) by univariate Cox proportional risk regression and Lasso regression, where patients in the low-risk group had better prognostic survival. The signature was highly effective in predicting the prognosis of CC patients (AUC > 0.7) and independent prognostic analyses have shown that the signature can be used as an independent prognostic factor. The Nomogram has shown to be stable and accurate, and therefore can be used relatively well to predict survival at 1-, 3- and 5-years in CC patients, providing additional options for prognosis prediction in CC.

Another important finding shows that this prognostic model is significantly related to the TME, confirming that pyroptosis plays a non-negligible role in the TME. More and more evidence shows that pyroptosis is particularly important for the formation of tumors and TME, especially the tumor immune microenvironment(30). Studies have confirmed that about 95% of cervical cancer patients may be caused by persistent infection with HPV, and the human immune system plays an important role in the infection response process, laying the foundation for immunotherapy of cancer(31).

This was confirmed in our study, which found significant differences in TME and immune function between the low- and high-risk groups, and patients with high TME scores having a better prognosis. This finding is consistent with previous studies, where patients with high TME scores had a stronger anti-tumor immune response, greater potential to benefit from immunotherapy, and longer survival(32, 33). In addition, correlation analysis showed that B cell and T cell CD8 + were negatively correlated with the risk scores, and neutrophils were positively correlated with the risk scores. Recent studies have shown that GSDME is a tumor suppressor that enhances the phagocytosis of tumor-associated macrophages and promotes the infiltration and activation of NK cells and CD8 + T lymphocytes, thereby inhibiting tumor growth(9). Xi et al. found that GSDMD was positively correlated with the expression levels of CD8A, GZMB, and IFNG in nonsmall cell lung cancer (NSCLC) tissues, and the expression was up-regulated in activated CD8 + T cells, enhancing the lethality of CD8 + T cells on NSCLC cells(34). Consistent with the result, Wang et al. found that the bio-orthogonal shear system applied to Gasdermin protein activated pyroptosis, reshaped the tumor immune microenvironment, and activated a strong T cell-mediated anti-tumor immune response, exerting a powerful anti-tumor effect(35). Tumor-associated neutrophils are involved in regulating tumor development, while IL-1β and IL-18 recruit neutrophils to tumor sites(36), and GSDMD induce neutrophil death(37). Neutrophils may be part of the local and systemic trigger of immune escape in cervical cancer cells. The increase in total neutrophil count in progressive cervical cancer inhibits the anti-tumor activity of T cells, thereby suppressing the immune action(38–40). At the same time, our study further confirmed that the expression of multiple immune checkpoints and m6A-related mRNAs differed significantly between the low- and high-risk groups. Recent studies have found that abnormal expression of immune checkpoints interferes with the tumor immune microenvironment and helps tumor cells evade immune destruction(41, 42). These studies all highlight the close association of the host immune response and microenvironment with the development of CC.

In our study, Granzyme B (GZMB), a member of the prognostic model, was significantly upregulated in CC tissues, and GZMB expression was also significantly upregulated in patients with advanced CC (Grade 3–4), and it was negatively associated with survival.

GZMB is a serine protease and a potentially versatile pro-inflammatory molecule that promotes the progression of different inflammatory diseases or cancers(43). GZMB is expressed in uroepithelial carcinoma, pancreatic cancer, and melanoma cells and promotes cancer cell invasion(44–46). Our study also found that GZMB was negatively associated with survival in BLCA and SKCM. GZMB has long been known for its activity in protein hydrolysis-mediated apoptosis, while little research has been done on its

role in pyroptosis. GZMB was found to be able to cleave GSDME and kill lymphocytes to activate pyroptosis, thus converting apoptosis to pyroptosis(9).

The GZMB/miR-378a/TRIM52-AS1 regulatory axis with a strong correlation to the development of CC was extracted from the mRNA-miRNA-LncRNA interaction network. The miR-378a (previously known as miR-378) is an important member of the microscopic non-coding RNA family. miR-378a has been reported to be aberrantly upregulated in HPV16/18 positive cervical cancer tissues, and elevated miR-378a expression may be induced by oncoprotein E6/E7(47). It has also been reported that miR-378a expression is elevated in cervical cancer tissues and cervical cancer cell lines, and may act through the ST7L/Wnt/β-catenin signaling pathway(48). It is also reported that lncRNA TRIM52-AS is under-expressed in renal cancer tissues. Overexpression of TRIM52-AS1 can significantly inhibit the growth and migration of renal cancer cells, suggesting that TRIM52-AS1 may be a potential oncogene(49). In our study, miR-378a and TRIM52-AS1 were significantly up-and down-regulated in CC, respectively, and CC patients with overexpression of TRIM52-AS1 had a better prognosis. Thus, the GZMB/ miR-378a/TRIM52-AS1 regulatory axis may play an important regulatory role in the development of CC. Our signature provides a potential target for targeted therapy of CC patients, especially GZMB.

Conclusions

We identified a prognostic signature and constructed a GZMB/miR-378a/TRIM52-AS1 regulatory axis based on PRGs, which is expected to provide theoretical support for the study of molecular mechanisms and prognostic assessment of cervical cancer. However, there are some limitations to our study, of which tumor heterogeneity is an issue that should not be overlooked, and still needs to be validated by more extensive in vivo and in vitro studies.

Declarations

Ethics approval and consent to participate

Not applicable.

Consent for publication

Not applicable.

Availability of data and material

The information of this study is obtained by the TCGA, UCSC Xena, Kaplan Meier-Plotter, Timer 2.0, String, TargetScan, miRTarBase, LncBase Predicted v.2, and StarBasedatabase database. We are grateful to them for the source of data used in our study.

Competing interests

The authors declare that they have no competing interests.

Funding

Not application.

Authors' contributions

Cankun Zhou and Yuhua Zheng performed data analysis work and aided in writing the manuscript. Cankun Zhou and Xiaochun Liu designed the study, assisted in writing the manuscript. Chaomei Li edited the manuscript. All authors read and approved the final manuscript.

Acknowledgements

Not application.

References

1. Ward ZJ,, et al. The role and contribution of treatment and imaging modalities in global cervical cancer management: survival estimates from a simulation-based analysis. Lancet Oncol. 2020;21:1089–98.
2. Cohen PA, Jhingran A, Oaknin A, Denny L. Cervical cancer. Lancet. 2019;393:169–82.
3. Ward ZJ, Scott AM, Hricak H, Atun R. Global costs, health benefits, and economic benefits of scaling up treatment and imaging modalities for survival of 11 cancers: a simulation-based analysis. Lancet Oncol. 2021;22:341–50.
4. Karki R, Kanneganti TD. Diverging inflammasome signals in tumorigenesis and potential targeting. Nat Rev Cancer. 2019;19:197–214.
5. Zheng Z, Li G. (2020) Mechanisms and Therapeutic Regulation of Pyroptosis in Inflammatory Diseases and Cancer. *Int J Mol Sci* 21.
6. Rathinam VA, Fitzgerald KA. Inflammasome Complexes: Emerging Mechanisms and Effector Functions. Cell. 2016;165:792–800.
7. Kolb R, Liu GH, Janowski AM, Sutterwala FS, Zhang W. Inflammasomes in cancer: a double-edged sword. Protein Cell. 2014;5:12–20.
8. Zhou Z, et al. (2020) Granzyme A from cytotoxic lymphocytes cleaves GSDMB to trigger pyroptosis in target cells. *Science* 368.

9. Zhang Z, et al. Gasdermin E suppresses tumour growth by activating anti-tumour immunity. Nature. 2020;579:415–20.
10. So D, et al. Cervical cancer is addicted to SIRT1 disarming the AIM2 antiviral defense. Oncogene. 2018;37:5191–204.
11. Fang Y, et al. Pyroptosis: A new frontier in cancer. Biomed Pharmacother. 2020;121:109595.
12. Latz E, Xiao TS, Stutz A. Activation and regulation of the inflammasomes. Nat Rev Immunol. 2013;13:397–411.
13. Ye Y, Dai Q, Qi H. A novel defined pyroptosis-related gene signature for predicting the prognosis of ovarian cancer. Cell Death Discov. 2021;7:71.
14. Nagy Á, Munkácsy G, Győrffy B. Pancancer survival analysis of cancer hallmark genes. Sci Rep. 2021;11:6047.
15. Wang X, Li M. Correlate tumor mutation burden with immune signatures in human cancers. BMC Immunol. 2019;20:4.
16. Yoshihara K, et al. Inferring tumour purity and stromal and immune cell admixture from expression data. Nat Commun. 2013;4:2612.
17. Li T, et al. TIMER2.0 for analysis of tumor-infiltrating immune cells. Nucleic Acids Res. 2020;48:W509-w514.
18. Li T, et al. TIMER: A Web Server for Comprehensive Analysis of Tumor-Infiltrating Immune Cells. Cancer Res. 2017;77:e108–10.
19. Finotello F, et al. Molecular and pharmacological modulators of the tumor immune contexture revealed by deconvolution of RNA-seq data. Genome Med. 2019;11:34.
20. Becht E, et al. Estimating the population abundance of tissue-infiltrating immune and stromal cell populations using gene expression. Genome Biol. 2016;17:218.
21. Hinshaw DC, Shevde LA. The Tumor Microenvironment Innately Modulates Cancer Progression. Cancer Res. 2019;79:4557–66.
22. Shulman Z, Stern-Ginossar N. The RNA modification N(6)-methyladenosine as a novel regulator of the immune system. Nat Immunol. 2020;21:501–12.
23. Wang L, et al. Association between IL1B gene and cervical cancer susceptibility in Chinese Uygur Population: A Case-Control study. Mol Genet Genomic Med. 2019;7:e779.
24. Cui G, Yuan A, Sun Z, Zheng W, Pang Z. IL-1β/IL-6 network in the tumor microenvironment of human colorectal cancer. Pathol Res Pract. 2018;214:986–92.
25. Liu Q, et al. Interleukin-1β promotes skeletal colonization and progression of metastatic prostate cancer cells with neuroendocrine features. Cancer Res. 2013;73:3297–305.
26. Dong GW, Do NY, Lim SC. Relation between proinflammatory mediators and epithelial-mesenchymal transition in head and neck squamous cell carcinoma. Exp Ther Med. 2010;1:885–91.
27. Stratakis CA. Cyclic AMP-dependent protein kinase catalytic subunit A (PRKACA): the expected, the unexpected, and what might be next. J Pathol. 2018;244:257–9.

28. Kastenhuber ER,, et al. DNAJB1-PRKACA fusion kinase interacts with β-catenin and the liver regenerative response to drive fibrolamellar hepatocellular carcinoma. Proc Natl Acad Sci U S A. 2017;114:13076–84.
29. Shao W, et al. The Pyroptosis-Related Signature Predicts Prognosis and Indicates Immune Microenvironment Infiltration in Gastric Cancer. Front Cell Dev Biol. 2021;9:676485.
30. Yu P, et al. Pyroptosis: mechanisms and diseases. Signal Transduct Target Ther. 2021;6:128.
31. Kwon MJ,, et al. Clinical implication of programmed cell death-1 ligand-1 expression in tonsillar squamous cell carcinoma in association with intratumoral heterogeneity, human papillomavirus, and epithelial-to-mesenchymal transition. Hum Pathol. 2018;80:28–39.
32. Pasini FS,, et al. A gene expression profile related to immune dampening in the tumor microenvironment is associated with poor prognosis in gastric adenocarcinoma. J Gastroenterol. 2014;49:1453–66.
33. Zeng D, et al. Gene expression profiles for a prognostic immunoscore in gastric cancer. Br J Surg. 2018;105:1338–48.
34. Xi G, et al. GSDMD is required for effector CD8(+) T cell responses to lung cancer cells. Int Immunopharmacol. 2019;74:105713.
35. Wang Q, et al. A bioorthogonal system reveals antitumour immune function of pyroptosis. Nature. 2020;579:421–6.
36. Jorgensen I, Lopez JP, Laufer SA, Miao EA. IL-1β, IL-18, and eicosanoids promote neutrophil recruitment to pore-induced intracellular traps following pyroptosis. Eur J Immunol. 2016;46:2761–6.
37. Kambara H, et al. Gasdermin D Exerts Anti-inflammatory Effects by Promoting Neutrophil Death. Cell Rep. 2018;22:2924–36.
38. Alvarez KLF,, et al. Local and systemic immunomodulatory mechanisms triggered by Human Papillomavirus transformed cells: a potential role for G-CSF and neutrophils. Sci Rep. 2017;7:9002.
39. Mishalian I, et al. Tumor-associated neutrophils (TAN) develop pro-tumorigenic properties during tumor progression. Cancer Immunol Immunother. 2013;62:1745–56.
40. Abakumova TV,, et al. (2014) [Cytokines profile and metabolic activity of neutrophils of peripheral blood when progressing neoplasma]. *Patol Fiziol Eksp Ter*. 86–90.
41. Saleh R, Toor SM, Sasidharan Nair V, Elkord E. Role of Epigenetic Modifications in Inhibitory Immune Checkpoints in Cancer Development and Progression. Front Immunol. 2020;11:1469.
42. Rotte A, Jin JY, Lemaire V. Mechanistic overview of immune checkpoints to support the rational design of their combinations in cancer immunotherapy. Ann Oncol. 2018;29:71–83.
43. Velotti F, Barchetta I, Cimini FA, Cavallo MG. Granzyme B in Inflammatory Diseases: Apoptosis, Inflammation, Extracellular Matrix Remodeling, Epithelial-to-Mesenchymal Transition and Fibrosis. Front Immunol. 2020;11:587581.
44. D'Eliseo D, et al. Granzyme B is expressed in urothelial carcinoma and promotes cancer cell invasion. Int J Cancer. 2010;127:1283–94.

45. D'Eliseo D, et al. Epitelial-to-mesenchimal transition and invasion are upmodulated by tumor-expressed granzyme B and inhibited by docosahexaenoic acid in human colorectal cancer cells. J Exp Clin Cancer Res. 2016;35:24.
46. Dufait I, et al. (2019) Perforin and Granzyme B Expressed by Murine Myeloid-Derived Suppressor Cells: A Study on Their Role in Outgrowth of Cancer Cells. *Cancers (Basel)* **11**.
47. Wang X, et al. microRNAs are biomarkers of oncogenic human papillomavirus infections. Proc Natl Acad Sci U S A. 2014;111:4262–7.
48. Li S, Yang F, Wang M, Cao W, Yang Z. miR-378 functions as an onco-miRNA by targeting the ST7L/Wnt/β-catenin pathway in cervical cancer. Int J Mol Med. 2017;40:1047–56.
49. Liu Z, Yan HY, Xia SY, Zhang C, Xiu YC. Downregulation of long non-coding RNA TRIM52-AS1 functions as a tumor suppressor in renal cell carcinoma. Mol Med Rep. 2016;13:3206–12.

Figures

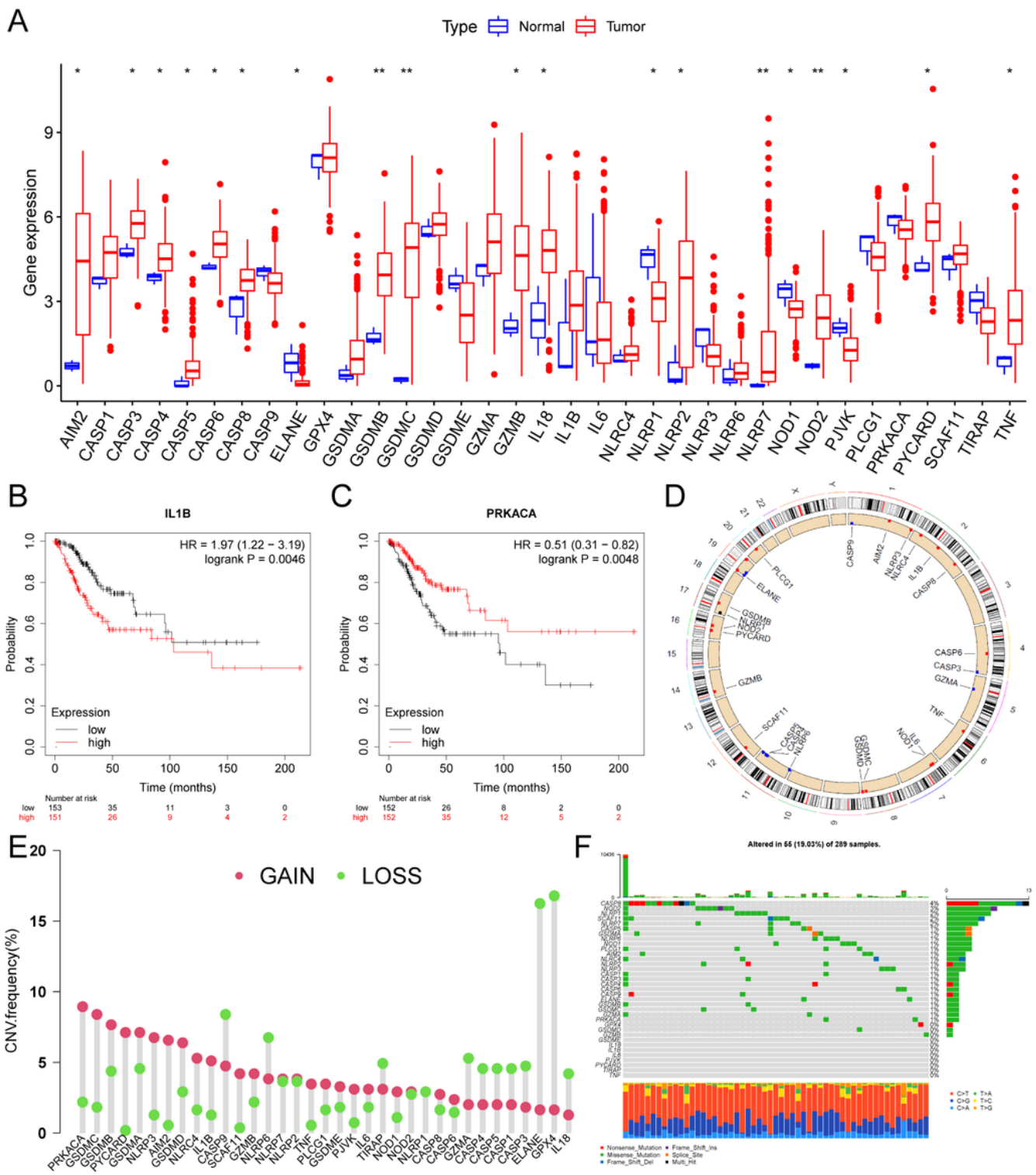

Figure 1

Expression and genetic variation landscape of PRGs in CC. (A) The boxplot demonstrated the expression of PRGs between normal and CC samples. Patients with low expression of IL 1B (B) and high expression of PRKACA (C) have more survival benefits. (D) Location of CNV alterations in PRGs on 23 chromosomes in CC cohort. (E) The CNV variation frequency of PRGs. The red and green dots represent CNV

amplification and deletion, respectively. (F9) Genetic alteration on a query of PRGs. PRGs, Pyroptosis-related genes. CC, Cervical cancer. CNV, Copy number variation.

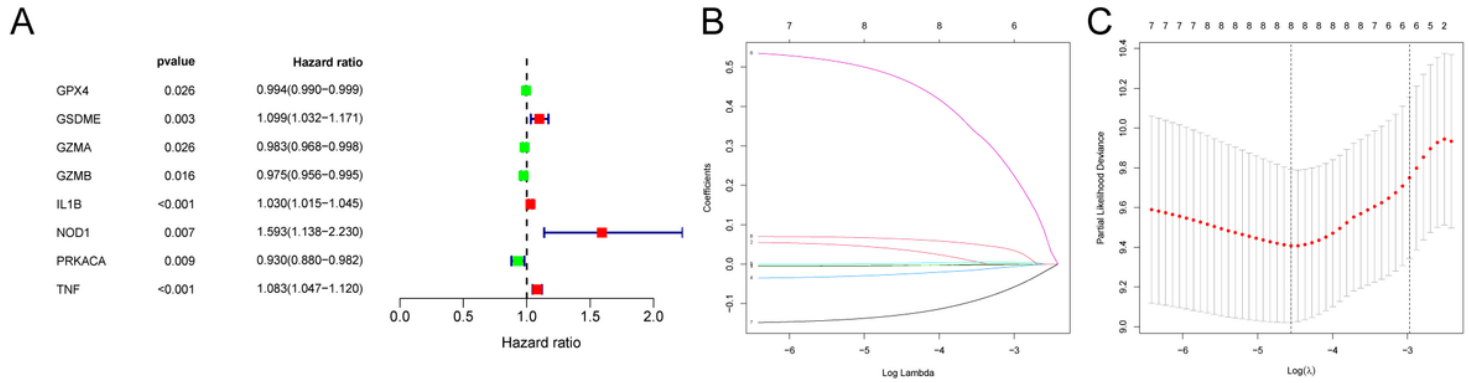

Figure 2

Screening for prognosis-related PRGs and LASSO regression. (A) Forest plot of the prognosis-related PRGs based on P < 0.05. Red and green indicate high and low risk, respectively. (B) LASSO coefficients for PRGs. Each curve represents a PRGs. (C) 1,000-fold cross-validation of variable selection in LASSO regressions by 1-SE criteria. PRGs, Pyroptosis-related genes. LASSO, Least absolute shrinkage and selection operator.

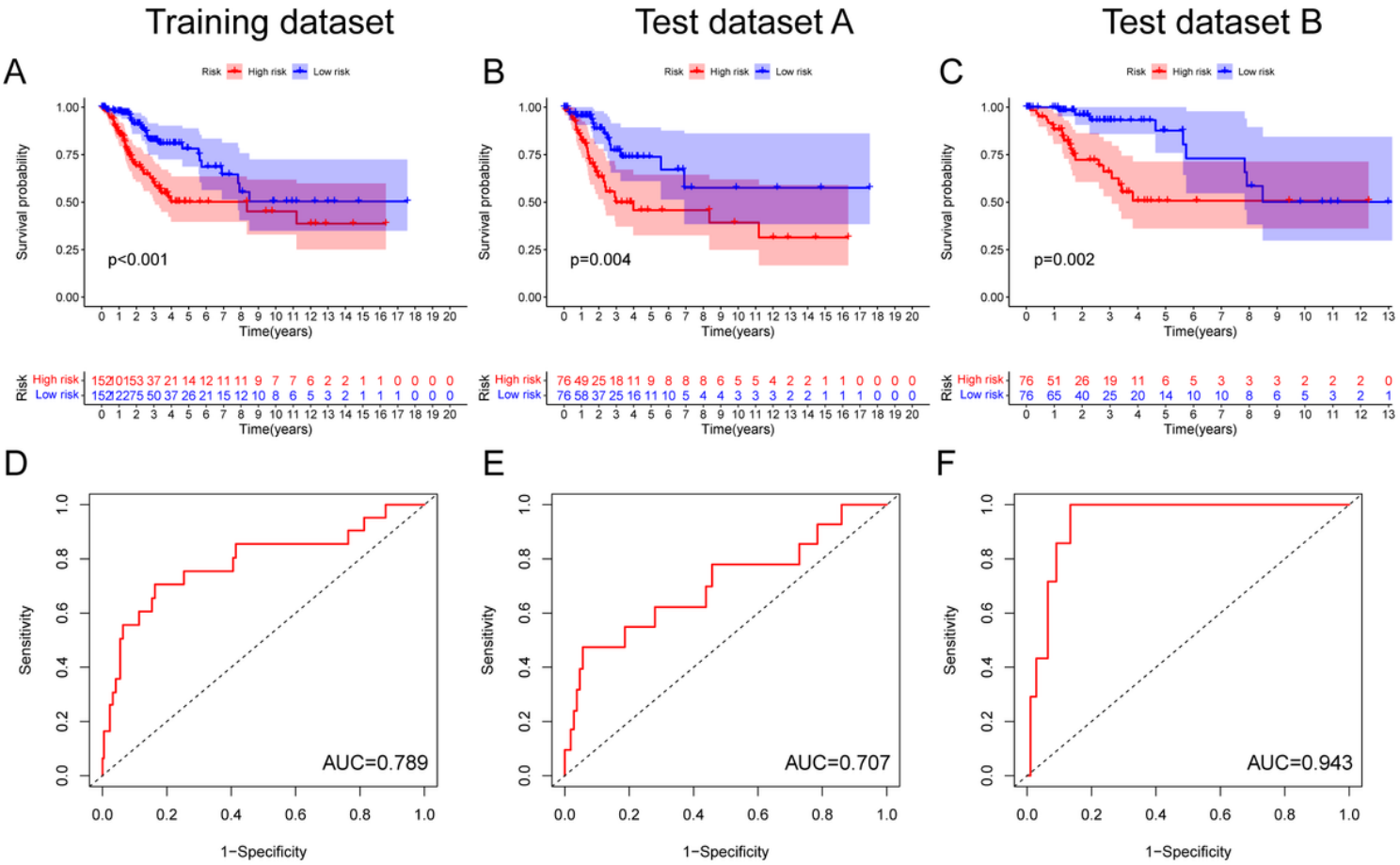

Figure 3

Construction and validation of the pyroptosis-related signature. (A/B/C) Kaplan-Meier curves showed lower overall survival rates in the high-risk group than in the low-risk group in the training dataset, test dataset A and test dataset B (P < 0.05). (D/E/F) The predicted ROC curves for the training dataset, test dataset A and test dataset B were 0.789, 0.707, and 0.943 respectively.

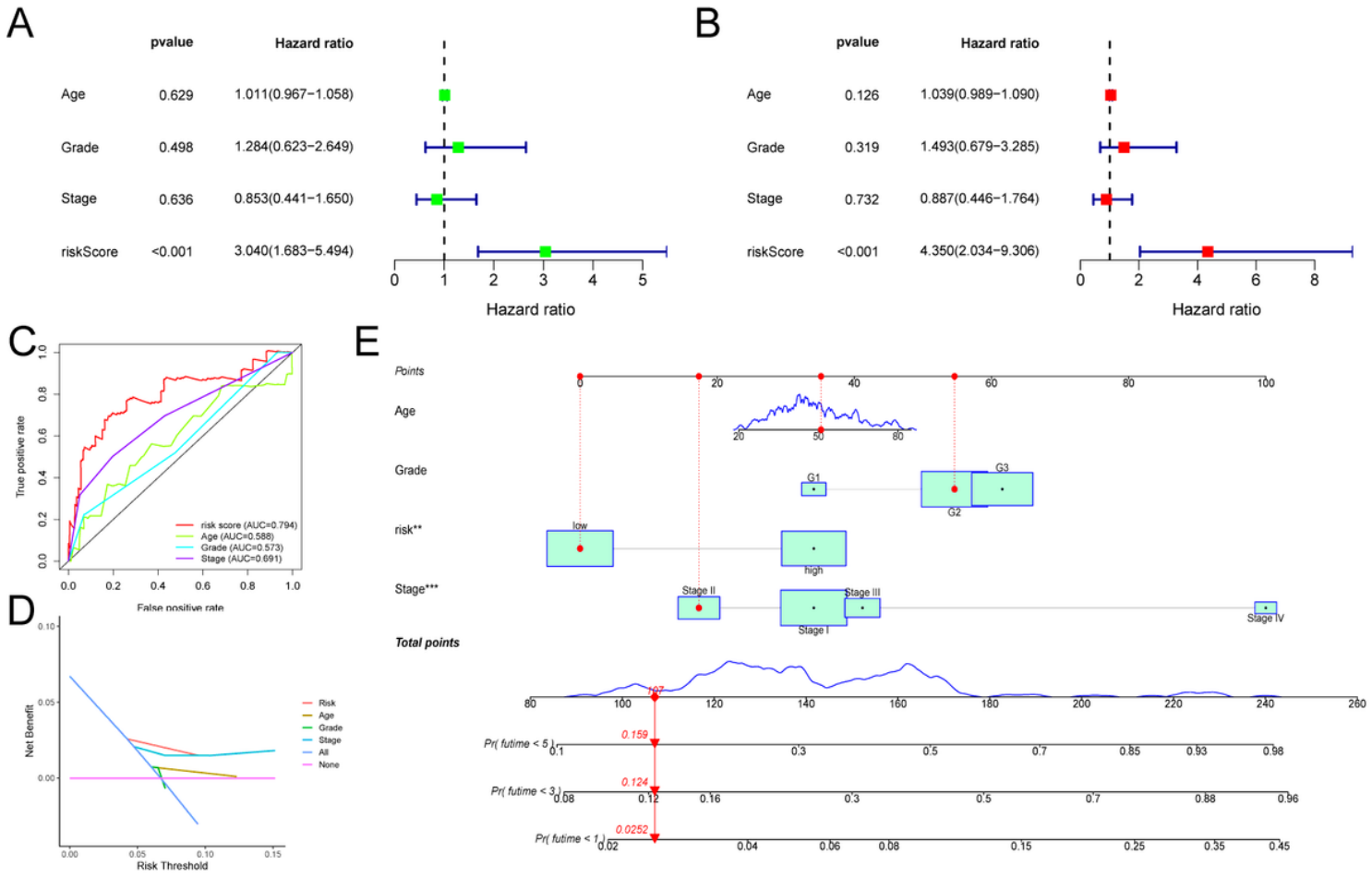

Figure 4

Prognostic value of the pyroptosis-related signature. (A/B) Univariate and multivariate COX analysis for the prognostic signature and clinical features (including Age, Stage, and Grade). (C) The AUC values of the prognostic signature and clinical features. (D) The DCA of the prognostic signature and clinical features. (E) Nomogram for both the signature and clinical features to predict 1-, 3- and 5-year survival rates.

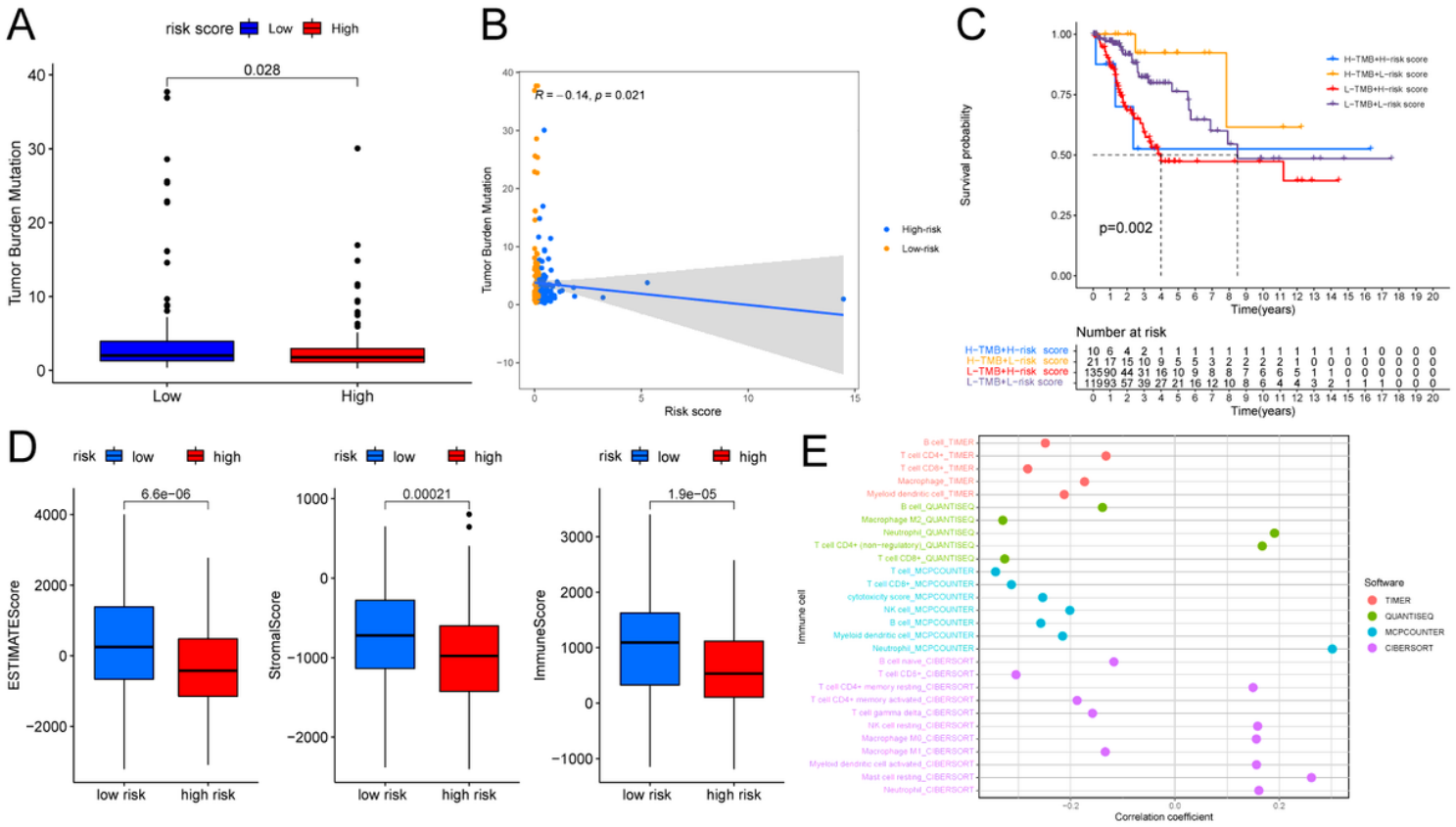

Figure 5

The relationship between the pyroptosis-related signature and the TMB, TME, and immune cell infiltration. (A) Patients in the high-risk group had lower TMB (P<0.05). (B) The correlation between risk score and TMB (R=-0.14, P<0.05). (C) Kaplan-Meier curves showed lower overall survival rates in the low-TMB combined with the high-risk group than in the other three groups(P<0.05). (D) The relationship between the risk score and TME, patients in the high-risk group had the lower stromal score, immune score, and estimate score(P<0.05). (E) The relationship between the risk score and immune cell infiltration is based on TIMER, QUANTISEQ, MCPCOUNTER, and CIBERSORT algorithm. Bubble plot for immune responses significantly associated with a risk score. TMB, tumor mutation burden. TME, tumor microenvironment.

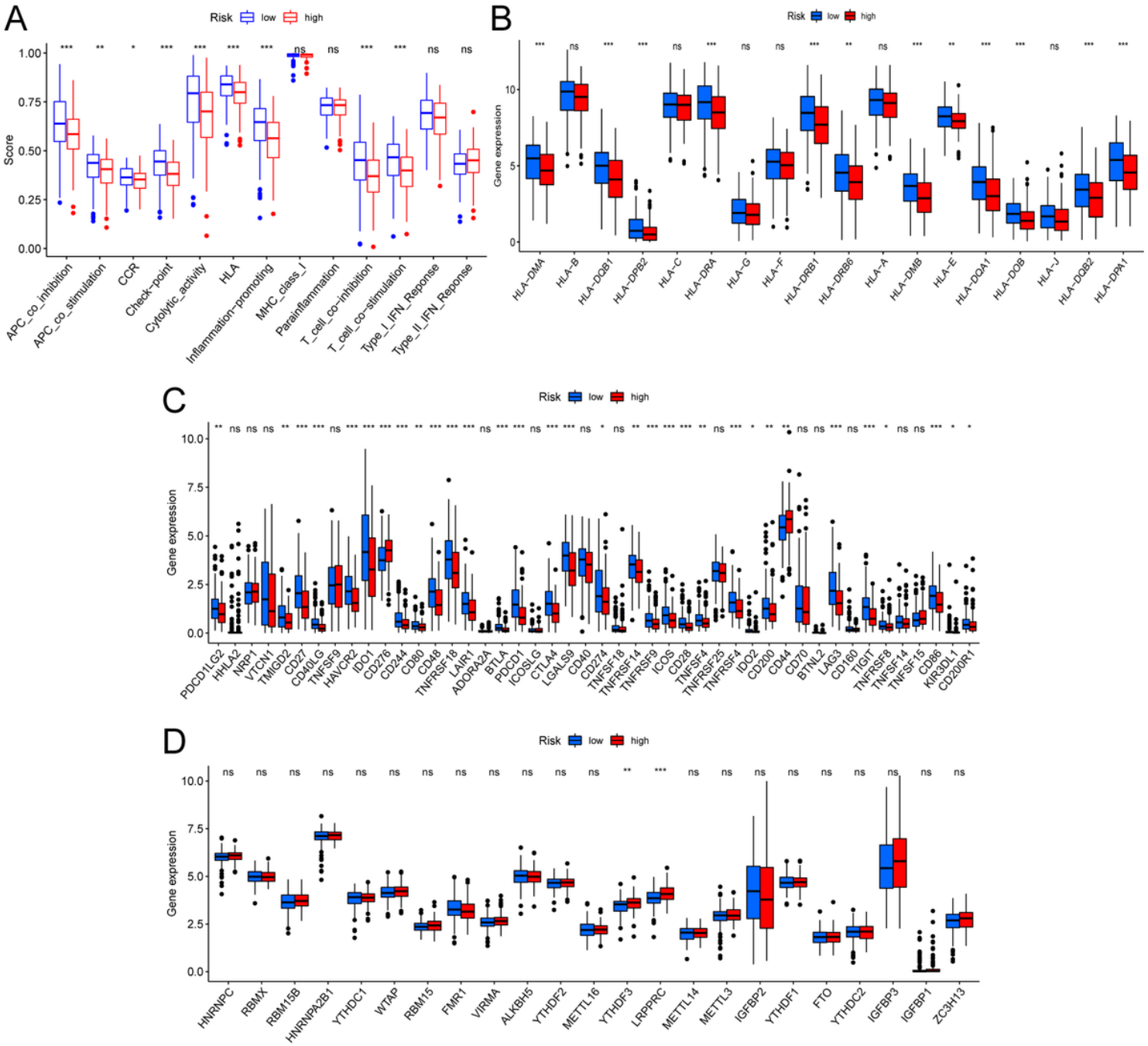

Figure 6

Diversity of immune microenvironment characteristics in high- and low-risk groups. (A) The activity differences of each immune function between high and low-risk groups. (B) The differences of each HLA-related gene between both risk groups. (C) The expression status of immune checkpoints between both risk groups. (D) The expression status of m6A-related genes between both risk groups

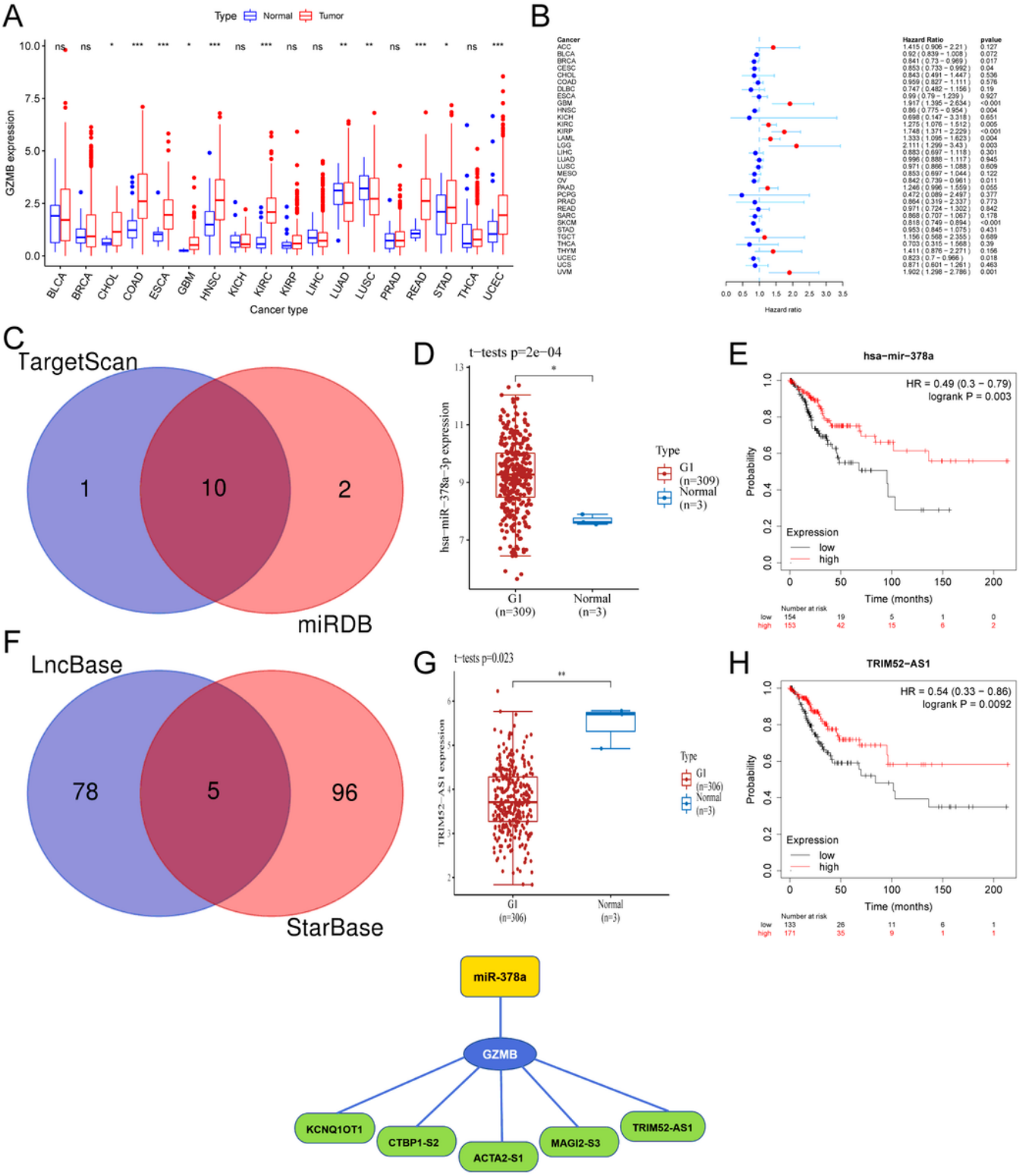

Figure 7

Pan-cancer analysis of core gene GEMB expression and survival prognosis, and associated ceRNA network construction. (A) Boxplot of GEMB differential expression between cancer and adjacent normal tissues. (B) Expression of GEMB correlates with overall survival in patients with different cancer types using univariate Cox proportional hazard regression models. (C) Venn diagram of miRNAs of TarBase and mirTarBase. The expression (D) and prognostic value (E) of miR-378a (Synonyms: miR-378a-3p) in

CC patients. (F) Venn diagram of LncRNAs of LncBase and StaBase. The expression (G) and prognostic value (H) of TRIM52-AS1 in CC patients. (I) Regulatory network mRNA-miRNA-LncRNA. CeRNA, competing endogenous RNA. CC, Cervical cancer.

Supplementary Files

This is a list of supplementary files associated with this preprint. Click to download.

- SupplementaryFigures.docx
- SupplementaryTable1.xlsx
- SupplementaryTable2.xlsx